

Tunable dispersion relations manipulated by strain in skyrmion-based magnonic crystals

Zhao-Nian Jin(金兆年), Xuan-Lin He(何宣霖), Chao Yu(于超), Henan Fang(方贺男), Lin Chen(陈琳), and Zhi-Kuo Tao(陶志阔)

Citation: Chin. Phys. B, 2024, 33 (**1**): 017501. DOI: 10.1088/1674-1056/acf03c
Journal homepage: http://cpb.iphy.ac.cn; http://iopscience.iop.org/cpb

What follows is a list of articles you may be interested in

Room-temperature creation and manipulation of skyrmions in MgO/FeNiB/Mo multilayers

Wen-Hui Liang(梁文会), Jian Su(苏鉴), Yu-Tong Wang(王雨桐), Ying Zhang(张颖), Feng-Xia Hu(胡凤霞), and Jian-Wang Cai(蔡建旺)

Chin. Phys. B, 2023, 32 (**12**): 127504. DOI: 10.1088/1674-1056/acf5d4

In-plane spin excitation of skyrmion bags

Shuang Li(李爽), Ke-Xin Li(李可欣), Zhao-Hua Liu(刘照华), Qi-Yuan Zhu(朱起源), Chen-Bo Zhao(赵晨博), Hu Zhang(张虎), Xing-Qiang Shi(石兴强), Jiang-Long Wang(王江龙), Rui-Ning Wang(王瑞宁), Ru-Qian Lian(连如乾), Peng-Lai Gong(巩朋来), and Chen-Dong Jin(金晨东)

Chin. Phys. B, 2023, 32 (**11**): 117503. DOI: 10.1088/1674-1056/acd327

Magnonic band-pass and band-stop filters with structurally modulated waveguides

Lai-He Feng(冯来和), Mang-Yuan Ma(马莽原), Zhi-Hua Liu(刘智华), Kai-Le Xie(解凯乐), and Fu-Sheng Ma(马付胜)

Chin. Phys. B, 2023, 32 (**6**): 067503. DOI: 10.1088/1674-1056/ac8afb

Gate-voltage control of alternating-current-driven skyrmion propagation in ferromagnetic nanotrack devices

Xin-Yi Cai(蔡心怡), Zhi-Hua Chen(陈志华), Hang-Xiao Yang(杨航霄), Xin-Yan He(何鑫岩), Zhen-Zhen Chen(陈珍珍), Ming-Min Zhu(朱明敏), Yang Qiu(邱阳), Guo-Liang Yu(郁国良), and Hao-Miao Zhou(周浩淼)

Chin. Phys. B, 2023, 32 (**6**): 067502. DOI: 10.1088/1674-1056/acb420

Magnetic triangular bubble lattices in bismuth-doped yttrium iron garnet

Tao Lin(蔺涛), Chengxiang Wang(王承祥), Zhiyong Qiu(邱志勇), Chao Chen(陈超), Tao Xing(邢弢), Lu Sun(孙璐), Jianhui Liang(梁建辉), Yizheng Wu(吴义政), Zhong Shi(时钟), and Na Lei(雷娜)

Chin. Phys. B, 2023, 32 (**2**): 027505. DOI: 10.1088/1674-1056/aca604

Tunable dispersion relations manipulated by strain in skyrmion-based magnonic crystals

Zhao-Nian Jin(金兆年)[1], Xuan-Lin He(何宣霖)[2], Chao Yu(于超)[2], Henan Fang(方贺男)[2], Lin Chen(陈琳)[2], and Zhi-Kuo Tao(陶志阔)[2,†]

[1] *Bell Honors School, Nanjing University of Posts and Telecommunications, Nanjing* 210003, *China*
[2] *College of Electronic and Optical Engineering & College of Flexible Electronics, Nanjing University of Posts and Telecommunications, Nanjing* 210003, *China*

(Received 9 June 2023; revised manuscript received 6 August 2023; accepted manuscript online 15 August 2023)

We theoretically investigate the propagation characteristics of spin waves in skyrmion-based magnonic crystals. It is found that the dispersion relation can be manipulated by strains through magneto-elastic coupling. Especially, the allowed bands and forbidden bands in dispersion relations shift to higher frequency with strain changing from compressive to tensile, while shifting to lower frequency with strain changing from tensile to compressive. We also confirm that the spin wave with specific frequency can pass the magnonic crystal or be blocked by tuning the strains. The result provides an advanced platform for studying the tunable skyrmion-based spin wave devices.

Keywords: skyrmion, magnonic crystal, spin wave, dispersion relation

PACS: 75.30.Ds, 75.80.+q, 85.70.Ay, 12.39.Dc **DOI:** 10.1088/1674-1056/acf03c

1. Introduction

Spin waves or corresponding quasiparticle magnons, as advanced information carriers, have attracted much attention in recent years.[1,2] Like semiconductors or photonic crystals, periodically modulated magnetic properties are realized in magnonic crystals, which can hold spin waves or magnons. By employing these periodically arranged structures, the dispersion relations of magnonic crystals can be customized to specific requirements. As a new emerging topologically magnetic texture, skyrmion has also shown the potential in realizing magnonic crystals.[3,4]

In 2009, magnetic skyrmion was experimentally observed in chiral magnet MnSi through neutron scattering by Mühlbauer *et al.*[5] Owing to the novel properties, skyrmion has shown strong potential applications in next-generation spintronic devices such as magnetic memory units with ultra-high density and logic gates with ultra-low power consumption.[6–9] Therefore, lots of researches of the dynamic properties driven by the electric current[10,11] or alternating microwave magnetic field have been conducted.[12,13] In 2012, spin-wave modes excited by microwave magnetic field in skyrmion crystal were predicted through numerical simulation.[12] Then, the magnetic excitations were observed experimentally in the helimagnetic insulator Cu_2OSeO_3.[13] The resonant modes are related to the external static magnetic field and material parameters such as Dzyaloshinskii–Moriya interaction (DMI) constant, and perpendicular magnetic anisotropy (PMA) constant.[14–16]

Recently, the skyrmion manipulated by using electrically generated mechanical strain has received much attention.[17,18] By considering the magnetoelastic coupling interaction, strain can be utilized to create skyrmions and annihilate skyrmions,and also modulate the configuration of stripe domains and skyrmions.[19–21] Additionally, from the applications of strain-induced surface acoustic waves (SAWs) another efficient method of generating and manipulating skyrmions has been found.[22–24]

Particularly, the periodical skyrmion arrangement can form magnon bands and bandgaps. Furthermore, the magnon band structure can be modulated by external effects such as magnetic fields and electric fields which will change the magnetic configuration of the skyrmion.[25–27] This dynamically modulated magnon band structure provides an advanced platform for studying tunable spintronics devices. In this work, we theoretically investigate the tunable dispersion relations manipulated by strain in skyrmion-based magnonic crystals. To start with, we analyze the phase diagram by changing strains and external static magnetic fields. Next, we calculate the dispersion relation curves under different strains and analyze the propagation properties of spin waves with specific frequencies.

2. Model and method

The dynamic behaviors of spin waves propagating in skyrmion-based magnonic crystals are simulated by the object oriented micromagnetic framework (OOMMF).[28] For a magnetic system, to obtain the dynamic response of its magnetic moment to time (the dynamic process), the Landau–Lifshitz–Gilbert (LLG) equation needs solving. The LLG equation can

†Corresponding author. E-mail: zktao@njupt.edu.cn

© 2024 Chinese Physical Society and IOP Publishing Ltd

be given as follows:

$$\frac{\partial \boldsymbol{m}(r,t)}{\partial t} = -\mu_0\gamma(\boldsymbol{m}(r,t)\times\boldsymbol{H}_{\rm eff}) + \alpha\left(\boldsymbol{m}(r,t)\times\frac{\partial \boldsymbol{m}(r,t)}{\partial t}\right), \tag{1}$$

where α is the Gilbert damping parameter, γ is the gyromagnetic ratio, μ_0 is the vacuum permeability, $\boldsymbol{m}(r,t)$ is the unit magnetization vector, and $\boldsymbol{H}_{\rm eff}$ is the effective magnetic field and can be expressed as

$$\boldsymbol{H}_{\rm eff} = -\frac{1}{\mu_0 M_{\rm s}}\frac{\partial E_{\rm tot}}{\partial \boldsymbol{m}(r,t)}, \tag{2}$$

where $M_{\rm s}$ denotes the saturation magnetization and $E_{\rm tot}$ is the total energy of a magnetic system. With magneto-elastic energy considered, the $E_{\rm tot}$ can be given by

$$E_{\rm tot} = E_{\rm ex} + E_{\rm PMA} + E_{\rm Ze} + E_{\rm demag} + E_{\rm DMI} + E_{\rm me}, \tag{3}$$

where $E_{\rm ex}$ is the exchange coupling energy, $E_{\rm PMA}$ is the perpendicular magnetic anisotropy (PMA) energy, $E_{\rm Ze}$ is the Zeeman energy, $E_{\rm demag}$ is the demagnetizing field energy, $E_{\rm DMI}$ is the DMI energy, and $E_{\rm me}$ is the magneto-elastic energy. Through the competition among these types of energy, different magnetic structures can be formed, and the ground state can be obtained by calculating the minimum value of the total energy.

In this work, the most important energy components are DMI energy and magneto-elastic energy. There are two types of DMI energy, namely, the interface DMI energy and bulk DMI energy. Here, the interface DMI energy is considered, which is given by

$$E_{\rm DMI} = D\left(\boldsymbol{m}\cdot\nabla m_z - m_z\nabla\cdot\boldsymbol{m}\right), \tag{4}$$

where D describes the strength of interfacial DMI. Magneto-elastic energy can be expressed as

$$E_{\rm me} = B_1\sum_{i=x,y,z} m_i^2\varepsilon_{ii} + B_2\sum_i\sum_{j\neq i} m_i m_i \varepsilon_{ij}. \tag{5}$$

Here, ε_{ij} is the strain tensor, and B_1 and B_2 are the magneto-elastic coupling constants.[29] In this work, biaxial in-plane strains are applied to a skyrmion-based magnonic crystal, so the strain tensor can be reduced to

$$\varepsilon = \varepsilon_{xx} = \varepsilon_{yy} = -\varepsilon_{zz}, \quad \varepsilon_{ij,i\neq j} = 0. \tag{6}$$

The typical material parameters for Co are used in the simulation, specifically, they being saturation magnetization $M_{\rm s} = 5.8\times10^5$ A/m, exchange stiffness constant $A_{\rm ex} = 1.5\times10^{-11}$ J/m, perpendicular anisotropy constant $K = 8\times10^5$ J/m^3, gyromagnetic ratio $\gamma = 2.211\times10^5$ m/(A·s), Gilbert damping coefficient $\alpha = 0.005$, magneto–elastic coupling constants $B_1 = -1.617\times10^7$ N/m^2 and $B_2 = 2.31\times10^6$ N/m^2.[30,31] The Co nano-layer is 2000 nm×100 nm×1 nm. The 2 nm×2 nm×1 nm mesh cell size is used to discretize the model and all simulations are performed at zero temperature.

3. Results and discussion

Firstly, our research focuses on examining the stability of a skyrmion-based magnonic crystal. Figure 1(a) illustrates the schematic diagram of our proposed device structure. In this structure, a biased voltage is applied to the piezoelectric layer in order to manipulate the strain in both of the piezoelectric layer and the skyrmion-based magnonic crystal layer. The simulated structure consists of a ferromagnetic (FM) ultrathin nano layer, a heavy metal layer (HM), and a bottom piezoelectric (PE) substrate. The Dzyaloshinskii–Moriya interaction generated by the FM/HM interface mainly results in the generation of skyrmions on the FM layer. Specifically, our proposed structure allows for the achievement of Neel-type skyrmions. In order to investigate the manipulation of skyrmions through strain, a voltage is applied to the PE layer, and the strain is generated owing to the converse piezoelectric effect. The length of the magnonic crystal is 2000 nm, the width is 100 nm, and the thickness of the magnonic crystal layer is 1 nm.

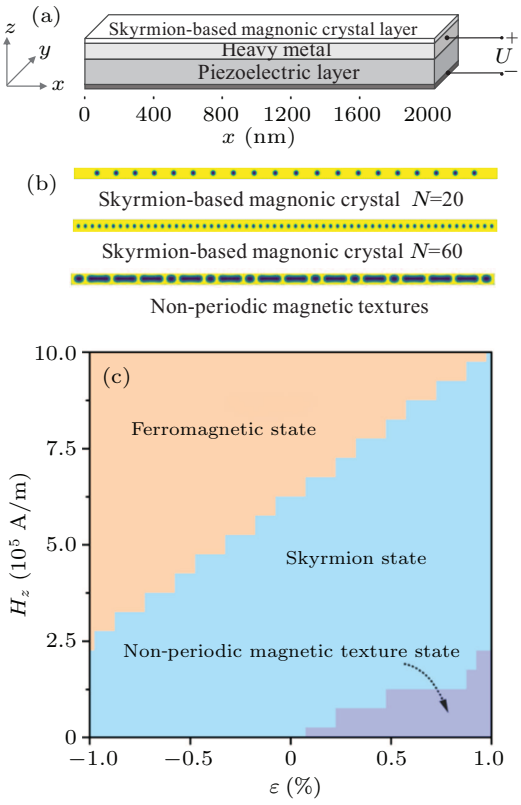


Fig. 1. (a) Schematic diagram of the proposed device structure. (b) Magnonic crystals with 20 and 60 skyrmions respectively, and non-periodic magnetic textures without strain. (c) Phase diagram of strain ε versus magnetic field H_z ($D = 4$ mJ/m^2).

By considering the interplay of various types of energy, including the magneto-elastic energy induced by the strain, different magnetic configurations can be achieved. Figure 1(b) shows the typical magnetic distributions. Skrymion-based

magnonic crystals with 20 and 60 skyrmions are presented with a periodic arrangement and controlled skyrmion size. Meantime, complex non-periodic magnetic textures can also be obtained by adjusting parameters such as DMI constant D, external static magnetic field H_z, and strain ε. In Fig. 1(c), we present the phase diagram of strain ε versus magnetic field H_z with D fixed at 4 mJ/m^2. It can be seen that ferromagnetic states are formed under higher magnetic field H_z and compressive strain (ε<0). With the decrease of the compressive strain and the increase of the tensile strain (ε>0), skyrmion states (or skyrmion-based magnonic crystals) can be formed. Also, non-periodic magnetic texture states are formed under higher tensile strain and lower magnetic field H_z. It is suggested that the voltage-induced strain can modulate the magnetic total energy via magneto-elastic coupling. On the other hand, the induced strain can also affect the magnetic anisotropy of the FM layer, which will be introduced to re-distribute the magnetic moments.

To excite spin wave in the magnonic crystal, a sine cardinal field,

$$H_z'(t) = H_{z0}' \frac{\sin[\omega(t-t_0)]}{\omega(t-t_0)}$$

with amplitude H_{z0}' = 100 A/m and cutoff frequency f = 100 GHz, is applied to a central area of 200 nm×100 nm×1 nm as depicted in Fig. 2(a). The excited spin waves with frequencies ranging from 0 GHz to 100 GHz travel to both sides of the x direction, *i.e.*, positive and negative x directions respectively. Then the fluctuations of magnetization ($\delta m_z(x,t) = m_z(x,t) - m_z(x,0)$) along the line from (0 nm, 50 nm, 1 nm) to (2000 nm, 50 nm, 1 nm) are collected during 10 ns as shown in Fig. 2(b). The color bar denotes the value of $\delta m_z(x,t)$. To determine the dispersion relation, a two-dimensional double fast Fourier transform is applied to the evolution of $\delta m_z(x,t)$.

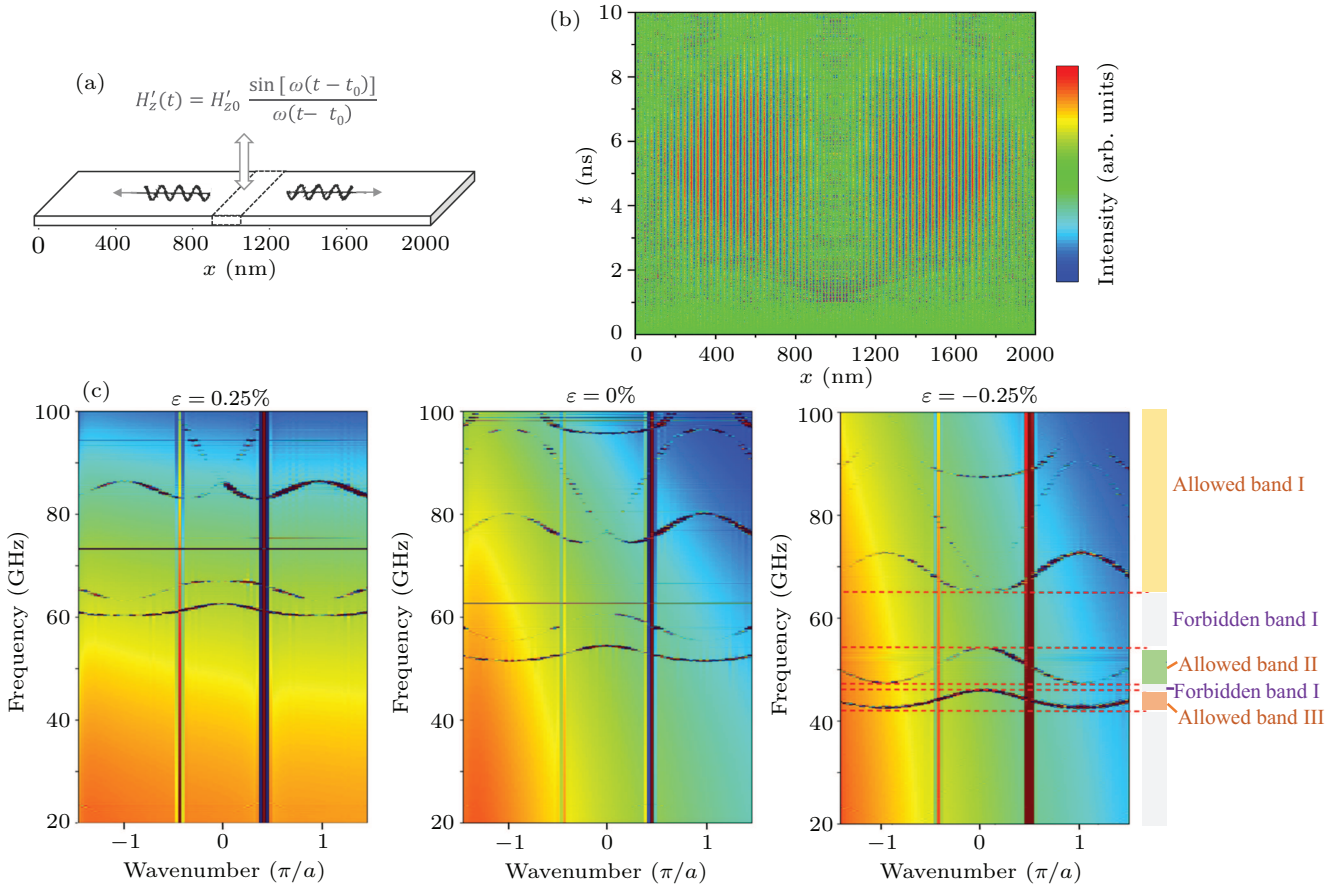


Fig. 2. (a) Schematic diagram for obtaining dispersion relations. (b) Fluctuations of magnetization $\delta m_z(x,t)$ without strain (N = 60, D = 3.5 mJ/m^2, $H = 5\times10^4$ A/m). (c) Dispersion relations in skyrmion-based magnonic crystals with strain ε = 0.25%, ε = 0, and ε = −0.25%, respectively, (N = 60, D = 3.5 mJ/m^2, $H = 5\times10^4$ A/m).

Figure 2(c) displays the dispersion relations observed in the skyrmion-based magnonic crystals under different strains: ε = 0.25%, ε = 0, and ε = −0.25%, which are represented by frequency versus wavenumber. It is known that different branches (modes) are presented in the dispersion relations due to the quantization of the wave vector across the strip width because a standing-wave pattern should form along the width direction of the strip.[25–27] Form Fig. 2(c), a periodic nature with folded branches can be seen, suggesting that the branch with the lowest frequencies corresponds to the uniform magnetization dynamics across the width of the strip (mode 1) while the upper one corresponds to the half-wavelength quantization (mode 2).[32] In the meantime, several allowed bands can be observed where spin waves can travel through the

magnonic crystals at specific frequencies and wavenumbers. Conversely, frequency ranges falling within the bandgaps (also referred to as forbidden bands, as indicated in Fig. 3(c)) prevent the spin waves from propagating through the magnonic crystal. Like the transport of electrons in solid crystals or photons in photonic crystals, the periodic modulation of magnetic properties introduced by the skyrmion lattice contributes to the tailoring of the dispersion relations.

An important finding in this study is that the dispersion relations can be manipulated by strain. As shown in Fig. 2(c), the dispersion relations shift toward higher frequencies when strain ε changes from -0.25% to 0.25%. Moreover, the ranges of frequencies within the allowed bands also vary with strain. This indicates that the strain has the ability to manipulate the distribution of magnetic texture through magneto-elastic coupling. In our proposed device, the configuration of periodically arranged skyrmions can be modulated by strain. Thus, the travelling characteristics of spin waves can be manipulated. Consequently, the strain-induced manipulation results in tunable dispersion relation, showcasing the potential for strain as a tool for manipulating and controlling the properties of spin waves.

Furthermore, we summarize the strain-dependent dispersion relations. Figures 3(a) and 3(c) illustrate the strain-dependent band characteristics inferred from dispersion relations for specific parameter values: $K = 8\times10^5$ J/m^3, $H = 5\times10^4$ A/m, $D = 3.5$ mJ/m^2; and $K = 2\times10^5$ J/m^3, $H = 1\times10^6$ A/m, and $D = 4$ mJ/m^2 respectively. Correspondingly, figures 3(b) and 3(d) show the variations of frequency variation range (Δf) with strain ε of the allowed and forbidden bands. It is evident that the allowed bands shift toward higher frequencies as the strain ε changes from -0.75% to 0.5%. In addition, the skyrmions are annihilated with strain $\varepsilon = 0.75\%$, as also depicted in Fig. 1(c). Furthermore, for different values of D, as shown in Figs. 3(a) and 3(c), the allowed bands exhibit the same strain-dependent characteristics.

In the meantime, it is worth noting that the strain not only causes the bands to shift toward higher frequencies, but also allows for manipulation of the frequency variation range within each band. As shown in Fig. 3(b), Δf of allowed band II decreases from about 9.8 GHz to 2.5 GHz with strain ε changing from -0.75% to 0.5%. Similarly, Δf of allowed band III decreases from about 4.8 GHz to 2.3 GHz. On the other hand, Δf of forbidden band I increases from about 5 GHz to 16 GHz with ε changing from -0.75% to 0.5%, whereas Δf of forbidden I decreases from about 2.6 GHz to 1.5 GHz with ε changing from -0.75% to -0.25% and keeps stable with ε increasing to 0.5%. Figure 3(d) presents similar characteristics for a different configuration of magnonic crystal.

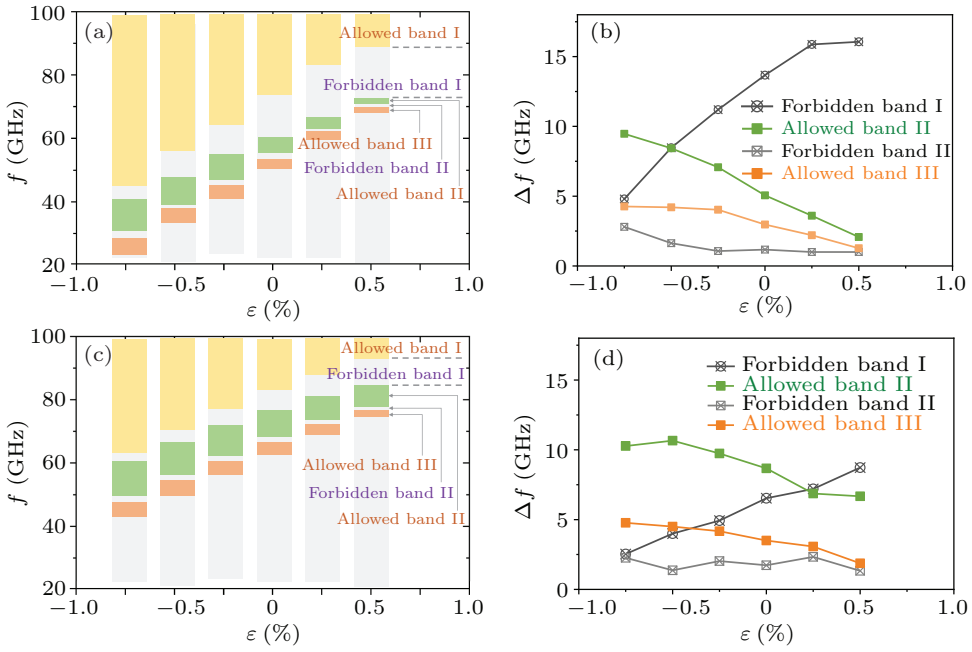


Fig. 3. Strain-dependent band characteristics inferred from dispersion relations for (a) $K = 8\times10^5$ J/m^3, $H = 5\times10^4$ A/m, $D = 3.5$ mJ/m^2, and (c) $K = 2\times10^5$ J/m^3, $H = 1\times10^6$ A/m, $D = 4$ mJ/m^2. Panels (b) and (c) display the corresponding frequency ranges of allowed and forbidden bands.

Next, we investigate the traveling behaviors of spin waves manipulated by strain. Figure 4(a) shows a schematic diagram for illustrating the process of exciting spin waves and capturing traveling behaviors. The spin wave is excited by a sinusoidal magnetic field along the z axis at frequency $f =$ 67 GHz, confined into the region 0 nm $< x <$ 100 nm, and then the evolution of average magnetization fluctuation δm_z at $x = 2000$ nm is collected for different strains: $\varepsilon = -0.25\%$, 0%, and 0.25%. In Fig. 4, it can be observed that fluctuation of magnetization δm_z at $x = 2000$ nm begins to exhibit signifi-

cant variations, respectively, at about 1.5 ns with $\varepsilon = -0.25\%$ and at about 1.7 ns with $\varepsilon = 0.25\%$. The corresponding velocities of spin waves are calculated to be 1267 m/s and 1117 m/s, respectively. This indicates that the strain can also manipulate the velocity of the spin wave. Additionally, very tiny magnetization fluctuations are observed in the absence of strain. This is consistent with the characteristics described in Fig. 3(a), where the frequency of 67 GHz falls within allowed band I for $\varepsilon = -0.25\%$ and allowed band III for $\varepsilon = -0.25\%$, while it falls within forbidden band II in the absence of strain.

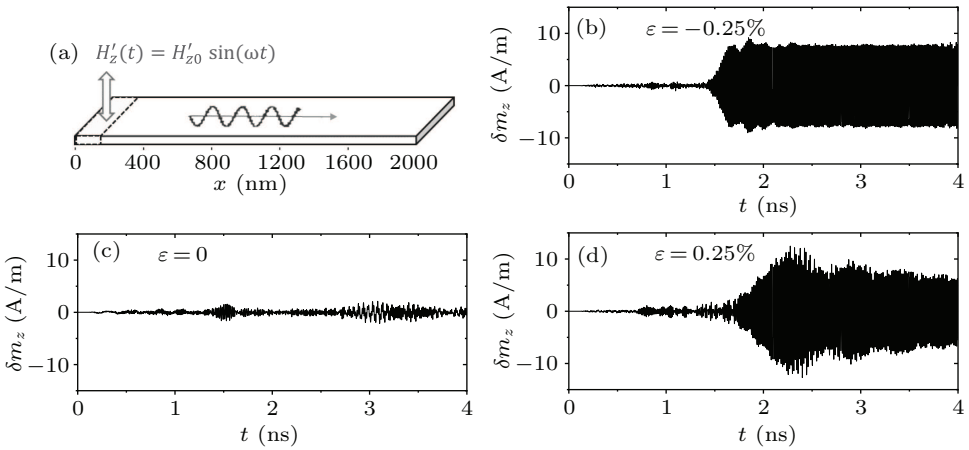


Fig. 4. (a) Schematic diagram for obtaining the traveling behaviors of spin waves. The fluctuations of magnetization δm_z at $H = 5 \times 10^4$ A/m, $D = 3.5$ mJ/m^2, $x = 2000$ nm, and $\varepsilon = -0.25\%$ (b), 0% (c), and 0.25% (d).

4. Conclusions

In summary, we investigated the tunable dispersion relations manipulated by strain in skyrmion-based magnonic crystals. Firstly, we calculated the phase diagrams of ground states under strains and external static magnetic fields, which show that the strain can induce different configurations such as FM state, skyrmion state, and complex non-periodic magnetic textures. Then, we studied the propagation properties of spin waves and calculated dispersion relation curves under different strains. It is found that the strain can manipulate the dispersion relations of skyrmion-based magnonic crystals through magneto-elastic coupling. Finally, we confirm that spin waves with specific frequencies can pass through the magnonic crystal or be blocked and that the on-off characteristics can be manipulated by strain. The results may provide a new idea for designing tunable spin wave devices based on skyrmion.

References

[1] Philipp P, Vitaliy I V, Alexander A S and Burkard H 2021 *Nat. Rev. Mater.* **6** 1114
[2] Krawczyk1 M and Grundler D 2014 *J. Phys.: Condens. Matter* **26** 123202
[3] Roldán-Molina A, Nunez A S and Fernández-Rossier J 2016 *New J. Phys.* **18** 045015
[4] Li Z Y, Ma M Y, Chen Z D, Xie K L and Ma F S 2022 *J. Appl. Phys.* **132** 210702
[5] Mühlbauer S, Binz B, Jonietz F, Pfleiderer C, Rosch A, Neubauer A, Georgii R and Böni P 2009 *Science* **323** 915
[6] Luo S J and You L 2021 *APL Mater.* **9** 050901
[7] Liu J H, Wang Z D, Xu T, Zhou H A, Zhao L, Je S G, Im M Y, Fang L and Jiang W J 2022 *Chin. Phys. Lett.* **39** 017501
[8] Puebla J, Kim J, Kondou K and Otani Y 2020 *Commun. Mater.* **1** 24
[9] Luo S J, Song M, Li X, Zhang Y, Hong J M, Yang X F, Zou X C, Xu N and You L 2018 *Nano Lett.* **18** 1180
[10] Iwasaki J, Mochizuki M and Nagaosa N 2013 *Nat. Nanotechnol.* **8** 742
[11] Peng L C, Karube K, Taguchi Y, Nagaosa N, Tokura Y and Yu X Z 2021 *Nat. Commun.* **12** 6797
[12] Mochizuki M 2012 *Phys. Rev. Lett.* **108** 017601
[13] Onose Y, Okamura Y, Seki S, Ishiwata S and Tokura Y 2012 *Phys. Rev. Lett.* **109** 037603
[14] Jin C D, Song C K, Wang J S, Xia H Y, Wang J B and Liu Q F 2017 *J. Appl. Phys.* **122** 223901
[15] Paikaray B, Joseph A, Murapaka C and Haldar A 2021 *J. Magn. Magn. Mater.* **529** 167900
[16] Xing L D, Hua D Y and Wang W W 2018 *J. Appl. Phys.* **124** 123904
[17] Kim J, Yang J, Cho Y J, Kim B and Kim S K 2018 *J. Appl. Phys.* **123** 053903
[18] Lonsky M and Hoffmann A 2020 *Phys. Rev. B* **102** 104403
[19] Qiu L, Shen L C, Zhang X C, Zhou Y, Zhao G P, Xia W X, Luo H B and Liu J P 2021 *Appl. Phys. Lett.* **118** 082403
[20] Vigo-Cotrina H and Guimarães A P 2020 *J. Magn. Magn. Mater.* **507** 166848
[21] Mehmood N, Wang J B, Zhang C L, Zeng Z Z, Wang J N and Liu Q F 2022 *J. Magn. Magn. Mater.* **545** 168775
[22] Shen X C, Zhao R Z, Ji L Z, Hu C L, Ren W L, Chen W C, Li Y X, Zhang J, Zhang X F and Dong X L 2022 *J. Magn. Magn. Mater.* **541** 168521
[23] Yang W G and Schmidt H 2021 *Appl. Phys. Rev.* **8** 021304
[24] Chen R Y, Chen C, Han L, Liu P S, Su R X, Zhu W X, Zhou Y J, Pan F and Song C 2023 *Nat. Commun.* **14** 4427
[25] Wang X G, Nie Y Z, Xia Q L and Guo G H 2020 *J. Appl. Phys.* **128** 063901
[26] Zhang C L, Jin C D, Wang J S, Xia H Y, Wang J N, Wang J B and Liu Q F 2019 *J. Magn. Magn. Mater.* **490** 165542
[27] Ma F S, Zhou Y, Braun H B and Lew W S 2015 *Nano Lett.* **15** 4029
[28] Beg M, Lang M and Fangohr H 2022 *IEEE Trans. Magn.* **58** 1
[29] Hu J M, Yang T N and Chen L Q 2019 *Acta Mater.* **183** 145
[30] Biswas A K, Ahmad H, Atulasimha J and Bandyopadhyay S 2017 *Nano Lett.* **17** 3478
[31] Zhu M M, Li Y T, Hu H M, Cui S T, Qiu Y, Yu G L and Zhou H M 2022 *Appl. Phys. Lett.* **121** 032402
[32] Kumar D, Dmytriiev O, Ponraj S and Barman1 A 2012 *J. Phys. D* **45** 015001